J. Electrochem. Sci. Eng. **15(1)** (2024) 2518; http://dx.doi.org/10.5599/jese.2518

Open Access : : ISSN 1847-9286
https://pub.iapchem.org/ojs/index.php/JESE

Original scientific paper

Al-Mg electrodeposition using chloride-based molten salts

Sreesvarna Bhaskaramohan[1], M. J. N. V. Prasad[2], G. V. Dattu Jonnalagadda[3] and Sankara Sarma V. Tatiparti[1,✉]

[1]*Department of Energy Science and Engineering, Indian Institute of Technology Bombay, Mumbai 400076, India*
[2]*Department of Metallurgical Engineering and Materials Science, Indian Institute of Technology Bombay, Mumbai 400076, India*
[3]*John F Welch Technology Centre, General Electric India Industrial Pvt. Ltd. Bangalore 560066, India*

Corresponding authors: ✉ *sankara@iitb.ac.in; Tel.: +91-22-2576-7672; Fax: +91-22-2576-4890*

Received: October 1, 2024; Accepted: November 9, 2024; Published: November 14, 2024

Abstract

Al-Mg alloys were potentiostatically electrodeposited from electrolyte with $AlCl_3$, NaCl, KCl and $MgCl_2$ at 180 °C for aircraft applications. The electrode setup includes a Cu cathode, Pt-mesh anode, and Al-rod pseudo-reference electrode. Cyclic voltammetry (CV) reveals the Al deposition sources as $Al_2Cl_7^-$ and $AlCl_4^-$. The Mg deposition source can be a reaction between $Al_2Cl_7^-$ and $MgCl_2$, and $MgCl_2$ dissociation (both releasing Mg^{2+}). Depositions at overpotentials: -1.03, -1.05, -1.06, and -1.10 V show current density-time curves with almost steady-state j, indicating planar diffusional growth. This is confirmed by layer-like morphologies with near-globular growth features. The average feature size decreases to -1.06 V and increases slightly at -1.10 V due to further deposition over the existing features. The deposit composition (Mg content) increases from 0.36 to 5.68 at.% from -1.03 to -1.10 V. Such a wide range of Mg content is obtained through minimal compositional changes in spent electrolytes, indicating the ease of less-noble Mg deposition. Al-Mg deposition scheme is devised with Al and Mg deposition perceived as $Al^{3+} + 3e^- \rightarrow Al$ and $Mg^{2+} + 2e^- \rightarrow Mg$; and $2Cl^- \rightarrow Cl_{2(\uparrow)} + 2e^-$ supplying electrons for deposition.

Keywords

Aluminum; magnesium; potentiostatic deposition; morphology; composition; scheme

Introduction

Aluminum (Al) - magnesium (Mg) alloys are very promising in aircraft applications due to their light weight and good corrosion resistance [1-5]. Al-Mg alloys have been conventionally produced through thermal processing, casting, conventional metal forming techniques, vapor phase deposition, *etc*. [6,7]. However, these methods of producing Al-Mg alloys incorporate defects such as internal, stresses, pores, and inhomogeneities in compositions and yield undesired morphologies, *etc*. [7].

Electrodeposition is a versatile technique for Al-Mg deposition due to its advantages, such as obtaining desired morphologies, uniform alloy composition, lower heat stress in the core alloy, and control over the thickness of the deposit [8]. Electrodeposition offers several parameters, such as potential/current, electrolyte composition, temperature, agitation, pH, *etc*, for achieving control over the deposit characteristics [9].

Electrodeposition of Al-Mg alloys is a challenge and has been attempted by only a few groups [9-18]. Aqueous electrolytes cannot be used for the electrodeposition of Al and Mg as the reduction potentials of Al (-1.67 V *vs.* NHE) and Mg (-2.356 V *vs.* NHE) are lower than that for water electrolysis ($E^{o}_{H_2O|OH}$= -0.828 V *vs.* NHE) [18]. Hence, water electrolysis occurs preferentially when attempting to deposit Al and Mg from aqueous solutions. Also, it is noteworthy that Al is nobler than Mg and, hence, can deposit preferentially over Mg. This creates a problem of not being able to deposit Mg to a desired composition when depositing Al and Mg together using non-aqueous electrolytes.

Electrodeposition Al and its alloys have been carried out using non-aqueous molten salts [13], ionic liquids [12,15-17,19], Grignard reagents [11], and organometallic electrolyte systems [9,10,18]. Due to their hygroscopic and/or moisture-sensitive nature, the non-aqueous electrolytes are handled in inert atmosphere conditions, which offers another challenge. In literature, deposition of a maximum of ~13.3 at.% Mg in Al-Mg alloys was reported by using ionic liquids by adding $AlCl_3$ to a 1,3-dialkyl--imidazolium chloride or benzene in the presence of tetrahydrofuran/crotyl alcohol [17]. Also, deposition cannot occur if the ionic liquid is basic [15]. Further, a clear trend of deposit compositions versus overpotentials/current densities is absent from these electrolyte systems [12,15-17,19]. In a work by Mayer, electrolytes comprising of NaF, KF, $Al(C_2H_5)_3$, $Al(C_2H_5)_3$, tri-iso-butyl-aluminum (iBu_3Al, where Bu = $-C_4H_9$) and $Mg(C_2H_5)_2$ prepared from Grignard reagents deposited Al-Mg alloys only if aluminum alkyl/magnesium alkyl mole ratio is $\geq$3.5, else pure Mg was deposited [11,20].

In our earlier extensive work on Al-Mg deposition from organometallic-based electrolytes, we reported the deposition of a wide range of compositions and morphologies of Al-Mg alloys by employing $Na[Al(C_2H_5)_4]$ + $2Na[(C_2H_5)_3Al\text{-}H\text{-}Al(C_2H_5)_3]$ + $2.5Al(C_2H_5)_3$ + 6toluene [18,21]. For example, morphologies with crystallographically consistent facets/feather-like morphology always possess 1 to 7 at.% Mg [22]. Smooth globular dendrites contain ~20 at.% Mg [21]. Rough globular dendrites, which always form over the smooth ones, possess ~65 to 80 at.% Mg [23]. Unfortunately, most of these electrolyte systems discussed here are very difficult to handle requiring extra precautions, are costly, and are banned in some countries.

Molten salt-based electrolytes, *e.g.* chloride-based, *etc.,* are relatively easier to handle, cheaper, and widely available in several countries. However, they are relatively less explored for the deposition of Al-Mg alloys, with systematic studies being scarce in the literature. For example, a stand-alone study by Li *et al.* [13] demonstrated Al-Mg composition in the range 2.41-9.14 at.% Mg using $AlCl_3$-$MgCl_2$-NaCl-KCl molten salt electrolytes. However, this system has yet to establish clear trends in Mg content with overpotential [13]. A trend of deposit compositions with overpotentials/current densities, relations between the compositions of deposits and electrolytes, and Al-Mg deposition schemes from molten salts are yet to be established. Most of the reported studies extensively deposited pure Al and its alloys (Al-Ti, Al-Sn, Al-Mn) on copper substrate.

In the present study, Al-Mg alloy films were deposited using a chloride-based molten salt electrolyte containing $AlCl_3$, NaCl, KCl, and $MgCl_2$ at 180 °C. Here, a copper (Cu) strip was used as the working electrode to deposit Al-Mg alloys to facilitate the direct comparison of the obtained results with those reported in the literature. Potentiostatic techniques with overpotentials of -1.03, -1.05, -1.06 and -1.10 V with respect to open circuit potential were used for deposition. The current density-

time (*j-t*) curves obtained from these depositions exhibit the typical characteristics and attain almost a steady-state current density, indicating planar diffusional growth (layer-like) of the deposits. This is confirmed by the morphologies of these deposits, which exhibit near-globular growth features in these Al-Mg layers. The average size of these features decreases up to -1.06 V. At -1.10 V, the size is slightly larger due to their growth by further deposition occurring over the already existing features. The composition (Mg content) of the deposits increases monotonously with the magnitude of overpotential. For example, 0.36 at.% Mg is obtained at -1.03 V and 5.68 at.% Mg is achieved at -1.10 V. This wide range of Mg content is achieved in the deposits through minimal changes in the spent electrolytes. This indicates that the present Al-Mg system has no obstacles to depositing less-noble Mg under the employed conditions. Also, a possible Al-Mg deposition scheme is devised by considering the electrochemical (from cyclic voltammetry) and non-electrochemical reactions in this system. The Al and Mg deposition can be perceived as $Al^{3+} + 3e^- \rightarrow Al$ and $Mg^{2+} + 2e^- \rightarrow Mg$ at the cathode. The electrons for these depositions are supplied by chlorine gas evolution (from CV) according to $2Cl^- \rightarrow Cl_{2(\uparrow)} + 2e^-$ at the anode.

Experimental

Electrodeposition of Al-Mg was conducted using a chloride-based molten salt electrolyte containing $AlCl_3$, NaCl, KCl, $MgCl_2$ (due to a non-disclosure agreement with the industry collaborators, the actual composition could not be revealed). Aluminium chloride (Reagent Plus®, 99 %) was procured from SIGMA; sodium chloride and potassium chloride (analysis grade) were purchased from EMPARTA; and magnesium chloride (anhydrous, ≥98 %) was obtained from SIGMA. Since the chemicals are moisture and oxygen-sensitive, they were handled in a glovebox (MBRAUN EASYlab^{pro}*i* 4-port) under argon (Ar) atmosphere, which maintained O_2 and moisture (H_2O) at < 0.1 ppm. These salts were melted together in the above-mentioned composition at 180 °C in a 10 ml beaker (electrochemical cell) to prepare the electrolyte. Several complexes can form in the electrolyte in its molten state. The complexes of Al, such as $Al_2Cl_7^-$ and $AlCl_4^-$ are well established in the literature [24-28]. However, the complexes of Mg are not established in the literature. Nevertheless, there are suggestions for forming complexes such as $Mg(AlCl_4)_2$ in the literature [24]. Also, $MgCl_2$ can combine with $Al_2Cl_7^-$ to form $AlCl_4^-$ and Mg^{2+}, according to Eqation (1) [15,16].

$$2Al_2Cl_7^- + MgCl_2^* \rightleftharpoons 4AlCl_4^- + Mg^{2+} \quad (1)$$

*Mg^{2+} can exist as complex

All the electrochemical experiments were conducted using a fresh stationary electrolyte at 180 °C in this cell and a CHI660E electrochemical workstation. A commercial Copper (Cu, 98 % pure, Patel) strip was used as the working electrode (WE). Prior to the experiments, this Cu strip was polished manually using sand papers (120C, 200C, 400C, 800C, 1000C, 2000C) followed by diamond paste (6 to 12 µm and 3 to 5 µm), alumina powder (1 µm) and finally by diamond paste (0.5 to 1 µm). Platinum mesh (Pt, 99.9 % pure, CH Instruments) was used as the counter electrode (CE), and an Aluminum (Al, 99.99 % pure, PureSynth) strip was employed as the pseudo-reference electrode (RE). The Al RE was polished using sandpapers (80C, 120C, 200C, 800C, 1000C) before employing it. Prior to the electrochemical experiments, open circuit potential (OCP) was measured. In order to identify various anodic activities such as Al-Mg dissolution, Cu dissolution and Cl_2 evolution, linear sweep voltammetry (LSV) was performed from OCP on (i) Cu strip with Al-Mg deposit on it, (ii) Pt rod with Al-Mg deposit on it and (iii) bare Pt rod. The results from these LSVs are shown in Figure 1(a). From Figure 1(a), the bare Pt rod substrate exhibits a signature of only Cl_2 evolution [29]. The Pt rod with an Al-Mg deposit on it, however, exhibits a wide anodic peak and plateau for Al-Mg dissolution [25,30] and for Cl_2

evolution [29], as indicated in Figure 1(a). From these results, the peaks for Al-Mg dissolution, Cu dissolution and Cl_2 evolution can be clearly distinguished in the LSV curve from the Cu strip with an Al-Mg deposit on it, as seen in Figure 1(a). Moreover, it must be noted that though Cu dissolution exhibits the highest activity (in terms of the current density), this anodic reaction would not happen during Al-Mg deposition on Cu. Cyclic voltammetry (CV) was performed by starting from OCP and between the switching potentials of -2.00 and +2.00 V *vs.* Al at a scan rate of 10 mV s^{-1}. The results of the potentiostatic electrodeposition experiments are reported here in terms of the overpotentials. The overpotentials were calculated as the difference between the applied potentials and OCP. The potentiostatic electrodeposition experiments were performed for 120 s at the applied potentials of -0.52, -0.55, -0.57 and -0.60 V *vs.* Al. These applied potentials correspond to the overpotentials of -1.03, -1.05, -1.06 and -1.10 V, respectively. Following the electrodeposition experiments, the WE were cleaned to remove any adhered solidified molten salt by ultrasonicating it in distilled water for 15 minutes. After every electrodeposition experiment, the spent electrolyte was transferred to an alumina crucible within the glove box. After the spent electrolyte in the crucible was solidified, it was brought outside the glovebox. The solidified spent electrolyte was handled in a fume hood by adding a few drops of water for neutralizing. The electrolyte was not disturbed until the end of fuming. Once the fuming ended, the spent electrolyte turned transparent and dried in a hot air oven at 120 °C. Eventually, this spent electrolyte was sent for compositional analysis.

Morphological and compositional analyses were performed on the deposits in as-deposited conditions on the Cu strip. For morphological analysis of the deposits, a JEOL FEG-SEM (JSM-7600F) scanning electron microscope (SEM) was employed in gentle beam-low (GB-L) mode. Compositional analysis was performed on both deposits and the spent electrolytes using an energy dispersive spectrometer (EDS) as an accessory to the SEM. The phase analysis was performed using Rigaku X-ray diffractometer (XRD, SmarLab 9 kW, Cu, $K\alpha$, λ = 0.15406 nm, 160 mA, 45 kV). The phases were indexed using ICSD code 44321.

Results and discussion

Cyclic voltammetry

Figure 1(b) shows the cyclic voltammogram for the electrodeposition of Al-Mg alloys from the employed molten salt. The scan begins from OCP (+0.48 V *vs.* Al) and eventually progresses into the cathodic segment towards -2.00 V *vs.* Al. The scan direction is shown by the arrows in Figure 1(b). While progressing in the cathodic segment, the scan exhibits a slight cathodic hump with a subtle peak at around -0.41 V *vs.* Al due to the Al deposition from $Al_2Cl_7^-$ according to Equation (2) [25-28].

$$4Al_2Cl_7^- \rightleftharpoons 7AlCl_4^- + Al^{3+} \quad (2)$$

Further progress of the scan results in another cathodic hump in the cathodic segment around a peak value of around -1.04 V *vs.* Al. This cathodic peak arises from the Al deposition from $AlCl_4^-$ according to Equation (3) [25-28].

$$AlCl_4^- \rightleftharpoons Al^{3+} + 4Cl^- \quad (3)$$

A careful observation suggests that the peak of Al deposition from $AlCl_4^-$ is relatively more pronounced than Al deposition from $Al_2Cl_7^-$. This suggests that the concentration of $Al_2Cl_7^-$ is possibly smaller (than that of $AlCl_4^-$) at the beginning of the CV. With the progress of CV, more $AlCl_4^-$ is produced according to Equations (1) and (2). This additionally produced $AlCl_4^-$, apart from its originally present concentration in the electrolyte, could lead to the pronounced peak for Al

deposition from $AlCl_4^-$. It should be noted that both $Al_2Cl_7^-$ and $AlCl_4^-$ can indulge in a non-electrochemical reaction according to Equation (4) to produce Cl^- [29,30].

$$2AlCl_4^- \rightleftharpoons Al_2Cl_7^- + Cl^- \quad (4)$$

The progress of CV towards negative potential beyond the Al deposition from $AlCl_4^-$ (Equation (3)) results in a steep increase in the current density to a very high value (Figure 1(b)), rendering an appearance of developing towards a large cathodic peak. However, such a cathodic peak is not attained by the time the scan reaches the negative switching potential of -2.00 V *vs.* Al. Hence, a trivial and partial reason for this large cathodic peak to be still in its developmental stage is that the scan was retracted towards a potential positive to the switching potential of -2.00 V *vs.* Al. The other reason this peak is still in its developmental stage is the deposition of Mg^{2+} from the electrolyte within these potentials. Mg can deposit from the employed chloride-based molten salt system according to Equation (1). Moreover, the possibility of Mg^{2+} deposition from un-complexed $MgCl_2$ according to Equation (5) [11,31-34] cannot be ruled out. From Figure 1(b), it is evident that the system did not reach diffusion limitation with respect to the concentration of Mg^{2+}, leading to this cathodic peak still being in its developmental stage.

$$MgCl_2 \rightleftharpoons Mg^{2+} + 2Cl^- \quad (5)$$

Upon retracting the CV scan in the anodic segment, the first prominent anodic peak was obtained at +0.45 V *vs.* Al (Figure 1).

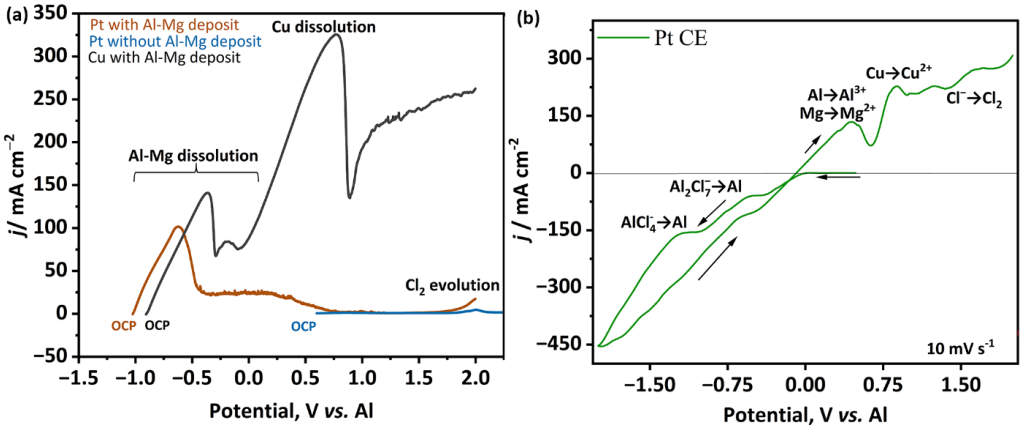

***Figure 1**. (a) Anodic linear sweep voltammetry curves from Pt substrates with and without Al-Mg deposit and Cu substrate with Al-Mg deposit on them. (b) Cyclic voltammogram on Cu using the present electrolyte system employing Pt CE*

This peak is asymmetric and arises due to the anodic dissolution of Al and Mg that were deposited in the cathodic segment. Further progress of the scan towards the potentials more positive this anodic dissolution of Al and Mg lead to the appearance of another anodic peak due to the dissolution of Cu from WE. At the potentials immediately adjacent to the Cu-dissolution peak, the CV flutters in a wavy form mainly due to the chlorine gas evolution according to Equation (6). The source of this chlorine gas are Equations (3) to (5) [29].

$$2Cl^- \rightarrow Cl_{2(\uparrow)} + 2e^- \quad (6)$$

Cyclic voltammetry was used in the present study to identify various electrochemical reactions that can take place in this system and to choose potentials for electrodeposition.

Potentiostatic electrodeposition of Al-Mg

The current density-time curves from the potentiostatic deposition experiments are shown in Figure 2(a). The obtained curves are typical of electrodeposition and exhibit the following

characteristic stages (i) a steeply rising feature in the current density values corresponding to (Al-Mg) nucleation events (ii) a decreasing current density after the peak corresponding to the overlapping of diffusion zones of these nuclei; (iii) an almost steady-state current density due to the planar diffusional growth of the deposits [35]. The *j-t* curve of the deposit at -1.10 V is not as flat as that of the rest of the deposits (Figure 2(a)). As expected, the peak and the steady-state current density values are generally higher at the higher overpotentials. The steady-state current density values are plotted against overpotential in Figure 2(b). The steady-state current density from the deposit at -1.10 V is way higher than that from -1.06 V. Those from deposits at -1.05 and -1.06 V are similar and higher than that from the deposit at -1.03 V. Figure 2(b) also shows a guideline delineating the expected morphologies for the chosen overpotentials in this study. The shape of the guideline and the expected morphologies are almost universal (irrespective of the system)[36]. However, the values of the overpotentials and the steady-state current densities spanning this guideline can depend on the alloy system being deposited [36]. From Figure 2(b), all the obtained steady-state current densities fall in the regime where layer-like or film morphology is expected.

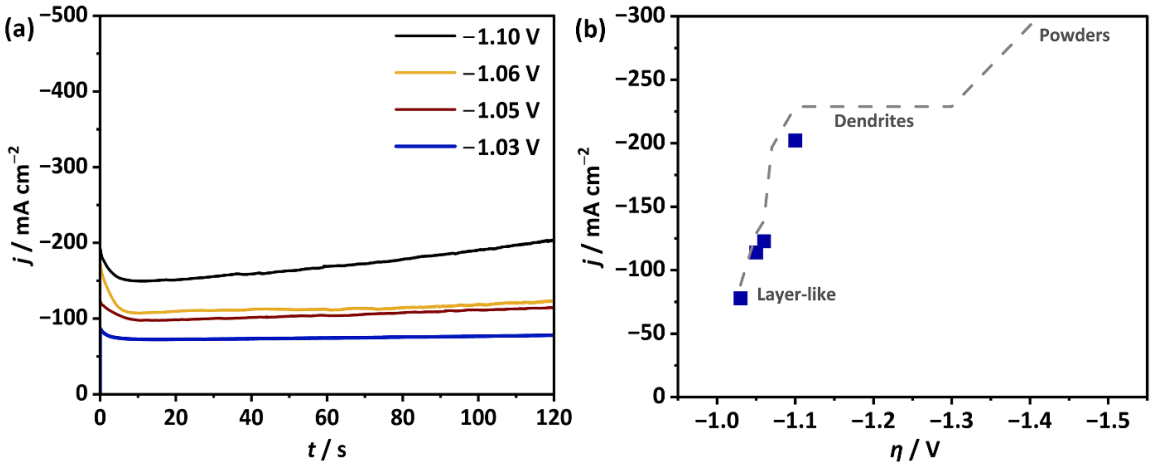

Figure 2. *(a) Current density - time curves of Al-Mg electrodeposition on Cu; (b) Steady-state current densities versus overpotential with guidelines delineating expected morphologies*

Morphologies, composition and phases of the Al-Mg deposits

The morphologies of all the deposits are shown in Figures 3(a)-(d) and possess near-globular features. The morphology within any given deposit is uniform as a consequence of potentiostatic deposition [37]. These morphologies represent the scenarios in the steady-state current density regimes since they are characterized at the end of the deposition. During the steady-state regime of the current density, the diffusion zones around the individual nuclei that were growing in the initial stages overlap, resulting in a blanket-like effect and ultimately yielding planar diffusion zones and growth. Such planar diffusional growth of morphologies offers good coverage on the substrate (*i.e.,* WE). For instance, the range of thickness obtained in the deposits is approximately between 350-500 nm. At such an advanced stage of the deposition (where planar, *i.e.,* film-like, growth is prevalent), the variation of morphology with thickness is expected to be very minimal, as seen here. However, the size of the near-globular features can change with the magnitude of the overpotential. For example, the obtained near-globular features are the coarsest in the deposit at -1.03 V and refine with the increase in the overpotential. The average size of these features (encircled in Figures 3(a) to 3(d)) is plotted as a function of overpotential in Figure 3(e). From Figure 3(e), it can be seen that the extent of the refinement of the features is the highest in the deposit at -1.06 V. From Figures 2(b) and 3(e), a significant increase in the steady-state current density from -1.03 to

-1.05 V leads to significant refinement in the feature size in the morphologies. Similarly, a small increase in the steady-state current density corresponding to the overpotentials from -1.05 to -1.06 V (Figures 2(b)) results in only a smaller extent of refinement in the average size of the features from these deposits. Interestingly, the average feature sizes are only slightly different in the deposits from -1.06 and -1.10 V, despite the very large difference in the steady-state current density between -1.06 and -1.10 V. This clearly shows that the average feature size is more sensitive to overpotentials up to -1.06 V, beyond which it becomes less sensitive. The reason for such a refinement up to -1.06 V is due to the increased charge transfer rate from -1.03 to -1.06 V. In addition, the number densities of the nuclei increase from -1.03 to -1.06 V, as more sites can get activated with an increase in the overpotential. The larger number density leads to the smaller feature size, as seen in Figure 3(e). In the deposit at -1.06 V, the density of the depositing nuclei is so high that no further nuclei can be accommodated beyond this overpotential. This leads to saturation in the number of nuclei depositing from -1.06 to -1.10 V. At -1.10 V, the additional energy supplied (*i.e.,* charge transfer) by the overpotential contributes to the growth of the near-globular features by further deposition over the already existing features.

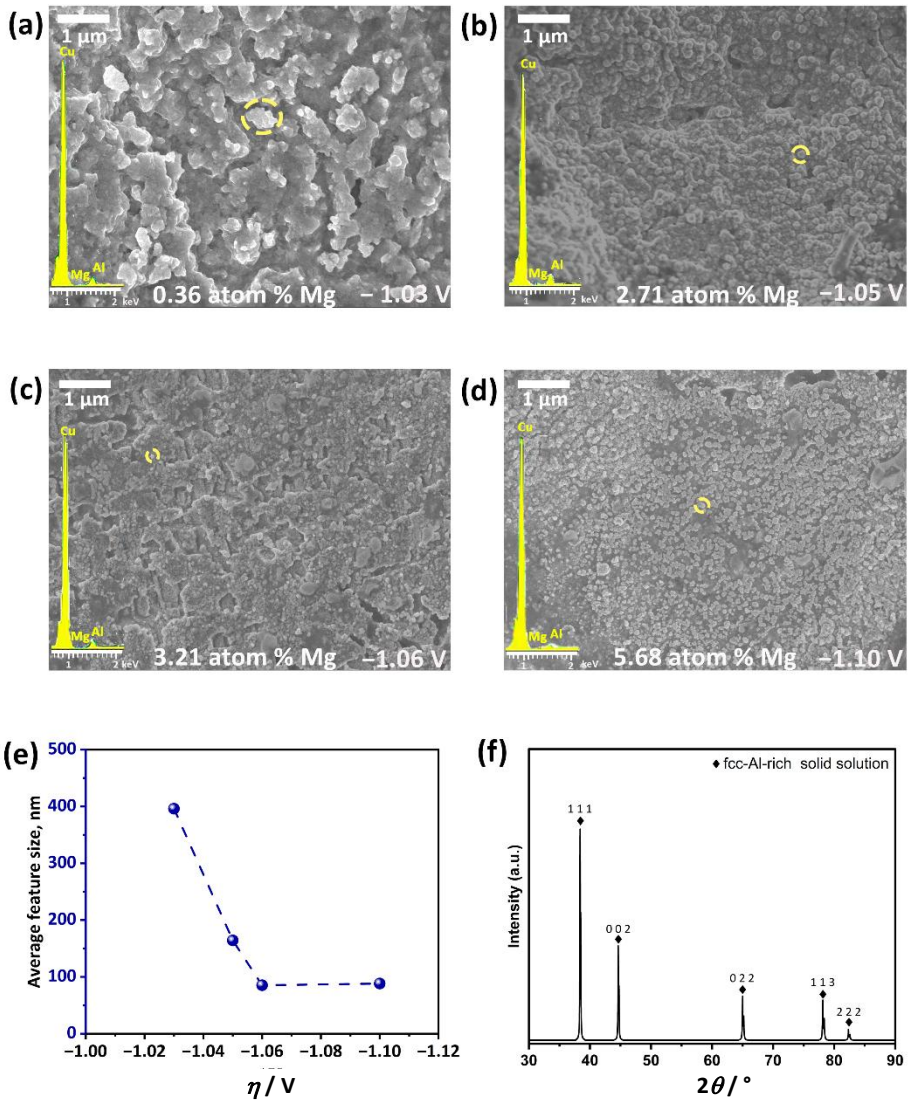

Figure 3. *Morphologies of deposits at overpotentials (a) -1.03 V, (b) -1.05 V, (c) -1.06 V, (d) -1.10 V (representative near-globular features encircled), (e) average feature size versus overpotential, (f) representative X-ray diffraction pattern of Al-Mg deposits*

This is probably because of the lower density of sites available for nucleation on the WE in this deposit for further nucleation events. This is why the *j-t* curve of the deposit is not as flat as that of the rest (Figure 2(a)). In fact, such a growth on the already existing features yields slightly coarsened near-globular features in the deposit at -1.10 V than that at -1.06 V (Figure 3(e)).

The compositions were analyzed from EDS spectra, which are embedded in the SEM images for the respective deposits. All the spectra show strong signals of Cu arising from the Cu substrate. The signals for Al and Mg can also be seen in these spectra. While estimating the composition in terms of Al and Mg, the contribution from Cu was neglected. Moreover, the absorption and fluorescence effects were also taken into consideration while estimating the compositions. As seen from Figures 3(a) to 3(d), the Mg content in the deposit increases with overpotential.

The XRD patterns of all the deposits are almost identical, with peaks corresponding to the face-centred cubic (fcc) phase. A representative XRD pattern from these deposits is shown in Figure 3(f). Hence, all the morphologies shown in Figure 3(a) to 3(d), containing compositions in the range of 0.36-5.68 at.% Mg, are supersaturated fcc-Al-rich solid solutions according to the equilibrium phase diagram of Al-Mg system [38]. This is expected as these deposits were obtained under highly non-equilibrium conditions, as evidenced by the high magnitudes of the current densities (Figure 2(a)).

Composition analysis

The Mg contents in the deposits and those in the spent electrolytes are plotted versus overpotential in Figure 4(a). From Figure 4(a), higher Mg is obtained in the deposits at the higher overpotentials. For example, the Mg content in the deposit at -1.03 V is 0.36 at.% and increases monotonously to 5.68 at.% in the deposit at -1.10 V. The standard reduction potentials of deposition ($E^{o}_{M^{+}|M}$, M =metal) of Al and Mg are -1.676 and -2.356 V *vs.* NHE, rendering Al nobler [39]. Hence, the deposition of the less-noble Mg is expected to be encouraged by overpotential, as is the case here (Figure 4(a)). Besides, the Mg content in the spent electrolyte does not significantly change with overpotential, as seen in Figure 4(a). In other words, a wide range of deposit compositions (*i.e.* Mg contents) can be obtained through minimal changes in the spent electrolyte compositions, as seen from the plot between the Mg content in the deposit versus that in the spent electrolyte in Figure 4(b).

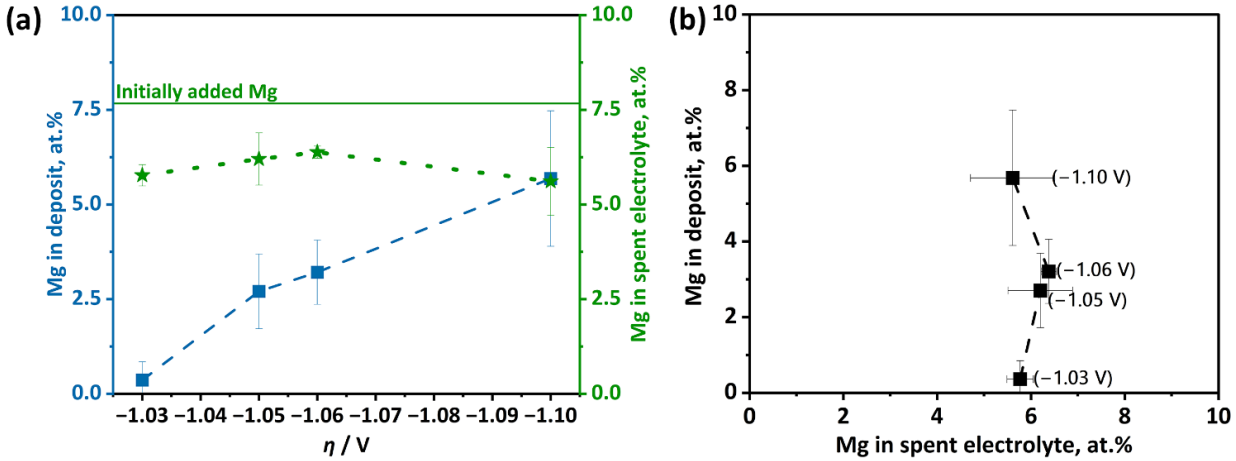

Figure 4. *(a) Mg in the deposit and spent electrolyte versus overpotential; (b) Mg in the deposit versus Mg in the spent electrolyte*

For clarity, the overpotentials at which the depositions were performed are also indicated in parentheses in Figure 4(b) adjacent to every point. This is a crucial result as it indicates that the present Al-Mg system does not encounter any obstacles to incorporating Mg in the deposits under

the employed conditions. Such ease in obtaining deposits with a wide range of Mg contents suggests that the deposition scheme can be simple.

Scheme of Al-Mg deposition

A possible scheme of Al-Mg deposition is devised by considering the initial composition of the electrolyte prior to the deposition, various electrochemical (deciphered from CV), and non-electrochemical reactions presented in Equations (1) to (5), and is shown in Figure 5. From the previous section, the deposition of Mg is envisaged as easy. The deposition of Al is, anyway, easy as it is a nobler metal, and its content in the deposits is much higher (Figures 4(a) and 4(b)).

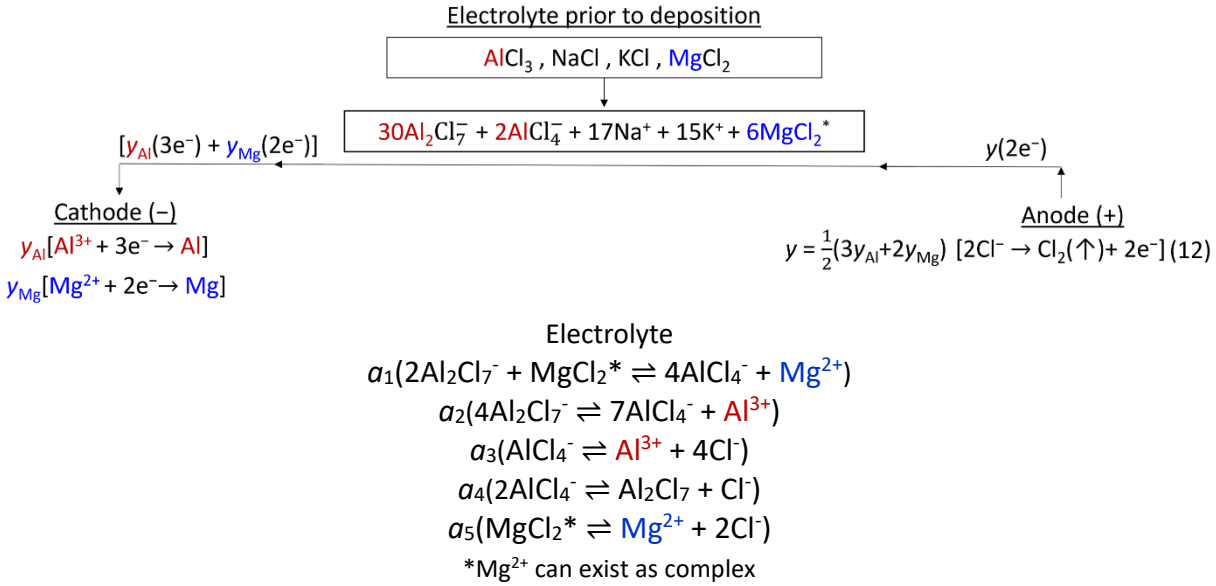

Figure 5. *Proposed scheme of Al-Mg electrodeposition using chloride-based molten salt electrolyte system employing Pt CE*

Hence, the electrochemical equations for the deposition of Al and Mg can be perceived as $Al^{3+} + 3e^- \rightarrow Al$ and $Mg^{2+} + 2e^- \rightarrow Mg$, both occurring at the cathode (Figure 5). Among all the electrochemical reactions perceived here, chlorine evolution (Figure 1) is the only anodic reaction (Figure 5). Hence, this is the reaction that supplies electrons for Al-Mg deposition. All the Equations (1) to (5) discussed above are shown in Figure 5. As mentioned earlier, it is assumed that $MgCl_2$ can combine with $Al_2Cl_7^-$ to form $AlCl_4^-$ and Mg^{2+}, according to Equation (1) [15,16]. Combined with Equation (5), this equation can serve as the source of Mg for its eventual deposition. The sources of Al for its deposition are Equations (2) and (3); and those for chlorine evolution are Equations (3) to (5), all occurring within the electrolyte (Figure 5). These reactions can happen to various extents in respective regions (*i.e.,* the electrodes and the electrolyte). The extents of reactions within the electrolyte are denoted with variables α_i (i = 1 to 5) in Figure 5. Those for Al and Mg deposition at the cathode are denoted as y_{Al} and y_{Mg}. Collectively, they are used to denote the extent of anodic reaction as y (Figure 5). Thus, Figure 5 represents the deposition scheme of Al-Mg alloys from the present chloride-based electrolyte system.

Conclusions

Al-Mg alloys with desired morphology and composition were potentiostatically electrodeposited from a chloride-based molten salt electrolyte containing $AlCl_3$, NaCl, KCl, and $MgCl_2$ at 180 °C for aircraft applications. The alloys were deposited on a Cu cathode (working electrode)

employing a Pt-mesh anode (counter electrode) and an Al rod as the pseudo-reference electrode. Prior to conducting the deposition experiments, cyclic voltammetry (CV) was performed to identify various electrochemical reactions in this system and to facilitate the choice of potentials for deposition. CV reveals that $Al_2Cl_7^-$ and $AlCl_4^-$ are the sources for depositing Al. Mg can deposit due to the reaction between $Al_2Cl_7^-$ and $AlCl_4^-$ (releasing Mg^{2+}) and the dissociation of $MgCl_2$ to Mg^{2+} and Cl^-. Eventually, potentiostatic deposition was performed for 120 s at overpotentials of -1.03, -1.05, -1.06 and -1.10 V with respect to open circuit potential. The current density-time curves exhibit the typical characteristics such as an initially rising *j-t* portion due to nucleation events, followed by a steeply dropping portion suggesting the overlapping of diffusion zones of these nuclei, and finally, an almost steady-state current density portion indicating the prevalence of planar diffusional growth of the deposits. The steady-state current densities fall in the regime of obtaining layer-like morphology. This is confirmed by the morphologies of the deposits, all of which exhibit near-globular growth features in the layers of Al-Mg alloys. The average size of these features decreases up to -1.06 V. At -1.10 V. However, the size increases slightly due to the growth of these features as further deposition occurs over the already existing features. The composition (Mg content) of the deposits increases monotonously with the magnitude of overpotential (*i.e.* 0.36 at.% at -1.03 V; 5.68 at.% at -1.10 V). Such a wide range of Mg content in the deposits is obtained through minimal changes in the spent electrolytes. This indicates that the present Al-Mg system does not encounter obstacles to incorporating less-noble Mg in the deposits under the employed conditions. A possible Al-Mg deposition scheme is devised by considering the electrochemical (from CV) and non-electrochemical reactions in this system. The Al and Mg deposition can be perceived as $Al^{3+} + 3e^- \rightarrow Al$ and $Mg^{2+} + 2e^- \rightarrow Mg$, both occurring at the cathode. The electrons for these depositions are supplied by chlorine gas evolution (from CV) according to $2Cl^- \rightarrow Cl_{2(\uparrow)} + 2e^-$, occurring at the anode.

Conflicts of interest: *The authors declare no conflict of interest.*

Acknowledgements*: Financial support from Department of Science and Technology, India and General Electric India Industrial Pvt. Ltd. under IMPRINT II C (File No.: IMP/2019/000241) is appreciated. FEG-SEM and EDS facilities at Sophisticated Analytical Instrument Facility (SAIF), IIT Bombay are acknowledged.*

References

[1] W. S. Miller, L. Zhuang, J. Bottema, A. J. Wittebrood, P. De Smet, A. Haszler, A. Vieregge. Recent development in aluminium alloys for the automotive industry. *Materials Science & Engineering A* **A280** (2000) 37-49. https://doi.org/10.1016/S0921-5093(99)00653-X

[2] E. Georgantzia, M. Gkantou, G.S. Kamaris. Aluminium alloys as structural material: A review of research. *Engineering Structures* **227** (2021) 111372 https://doi.org/10.1016/j.engstruct.2020.111372

[3] S. V. Kozhukharov, C. Girginov, S. Portolesi, A. Tsanev, V. Lilova, M. Georgieva, E. Lilov, P. Petkov. Sealing of cerium oxide coating primers on anodized AA2024-T3 alloy by boiling in Lourier buffers. *Journal of Electrochemical Science and Engineering* **14** (2024) 559-582. https://doi.org/10.5599/jese.1949

[4] C. Kammer, *Aluminum and aluminum alloys,* in *Springer Handbook of Materials Data*, W. Martinessen, H. Warlimont, Eds., Springer Nature, Switzerland, 2018, p. 157 https://doi.org/10.1007/978-3-319-69743-7

[5] K. K. Sankaran, R. S. Mishra, *Metallurgy and Design of Alloys with Hierarchical Microstructures,* Elsevier, 2017, p. 57. ISBN 978-0-12-812068-2

[6] M. Leary, Materials selection and substitution using aluminium alloys, in Fundamentals of Aluminium Metallurgy: Production, Processing and Applications, M. Leary, Ed., Woodhead Publishing Limited, 2010, p. 784 https://doi.org/10.1533/9780857090256.3.784
[7] I. C. Park, S. J. Kim. Electrochemical characteristics in seawater for cold thermal spray-coated Al-Mg alloy layer, *Acta Metallurgica Sinica (English Letters)* **29** (2016) 727-734 https://doi.org/10.1007/s40195-016-0437-7
[8] M. Ueda. Overview over studies of electrodeposition of Al or Al alloys from low temperature chloroaluminate molten salts. *Journal of Solid State Electrochemistry* **21** (2017) 641-647 https://doi.org/10.1007/s10008-016-3428-8
[9] S.S. V. Tatiparti, F. Ebrahimi. An understanding of the electrodeposition process of Al-Mg alloys using an organometallic-based electrolyte. *Journal of Applied Electrochemistry* **40** (2010) 2091-2098 https://doi.org/10.1007/s10800-010-0190-y
[10] H. Lehmkuhl, K. Mehler, B. Reinhold, H. Bongard, B. Tesche. Deposition of Aluminum-Magnesium Alloys from Electrolytes Containing Organo-Aluminum Complexes. *Advances in Engineering Materials* **3** (2001) 412-417 https://doi.org/1438-1656/01/0606-0412
[11] A. Mayer. Electrodeposition of Aluminum, Aluminum/Magnesium Alloys, and Magnesium from Organometallic Electrolytes. *Journal of the Electrochemical Society* **137** (1990) 2806-2809. https://doi.org/10.1149/1.2087078
[12] M. Morimitsu, T. Tanaka, M. Matsunaga, *Electrodeposition of Al-Mg Alloys from Lewis acidic $AlCl_3$-EMIC-$MgCl_2$ room temperature molten salts*, Electrochemical Society Proceedings Series, Molten Salts XIII: Proceedings of the international symposium, United States of America, 2002, p. 671-676. https://www.electrochem.org/dl/ma/201/pdfs/1459.pdf
[13] Y. Li, P. Zhao, Y. Dai, M. Yao, H. Gan, W. Hu. Electrochemical deposition of Al-Mg alloys on tungsten wires from $AlCl_3$-NaCl-KCl melts. *Fusion Engineering and Design* **103** (2016) 8-12 https://doi.org/10.1016/j.fusengdes.2015.11.053
[14] M. Morimitsu, N. Tanaka, M. Matsunaga. Induced Codeposition of Al-Mg Alloys in Lewis acidic $AlCl_3$-EMIC room temperature molten salts. *Chemistry Letters* (2000) 1028-1029. https://doi.org/10.1246/cl.2000.1028
[15] M.R. Ali, A. P. Abbott, K.S. Ryder. Electrodeposition of Al-Mg Alloys from Acidic $AlCl_3$-EMIC-$MgCl_2$ room temperature ionic liquids. *Journal of Electrochemistry* **21** (2015) 172-180 https://doi.org/10.13208/j.electrochem.140603
[16] H-M. Kan, S-S. Zhu, N. Zhang, X-Y. Wang. Electrodeposition of aluminum and aluminum—magnesium alloys at room temperature. *Journal of Central South University* **22** (2015) 3689-3697 https://doi.org/10.1007/s11771-015-2911-1
[17] L. Shen, B. Cui, S. Li, Y. Lei, Z. Shi. Electrodeposition of Al-Mg coating in the electrolyte system of C_4H_8O-C_6H_6-$LiAlH_4$-$AlCl_3$-MgX_2 (X=Cl, Br). *Journal of Materials Research and Technology* **22** (2023) 1349-1361 https://doi.org/10.1016/j.jmrt.2022.12.018
[18] S.S.V. Tatiparti, F. Ebrahimi. Electrodeposition of Al-Mg alloy powders. *Journal of the Electrochemical Society* **155** (2008) D363-D368 https://doi.org/10.1149/1.2885016
[19] X. Zhang, A. Liu, F. Liu, Z. Shi, B. Zhang, X. Wang. Electrodeposition of aluminum-magnesium alloys from an aluminum-containing solvate ionic liquid at room temperature. *Electrochemical Communications* **133** (2021) 107160 https://doi.org/10.1016/j.elecom.2021.107160
[20] A. Mayer, Electrodeposition of aluminum, aluminum/magnesium alloys, and magnesium from organometallic electrolytes, *1. international congress on high-tech-materials and finishing*, Berlin, F.R. Germany, 12 -14 March 1989, pp. 1-11. https://www.osti.gov/servlets/purl/6418518

[21] S. S. V. Tatiparti, F. Ebrahimi. The formation of morphologies and microstructures in electrodeposited nanocrystalline Al-Mg alloy powders. *Journal of The Electrochemical Society* **157** (2010) E167-E171 https://doi.org/10.1149/1.3468939
[22] S. S. V. Tatiparti, F. Ebrahimi. Preferred orientation and shape of electrodeposited nanocrystalline Al-Mg alloy dendrites. *Materials Letters* **65** (2011) 1915-1918 https://doi.org/10.1016/j.matlet.2011.04.018
[23] S. S. V. Tatiparti. Extended solubility in the electrodeposited nanocrystalline Al-Mg alloy dendrites. *Materials Letters* **65** (2011) 3173-3175 https://doi.org/10.1016/j.matlet.2011.06.112
[24] G. R. Stafford, T. Tsuda, C. L. Hussey. The structure of electrodeposited aluminum alloys from chloroaluminate ionic liquids: Let's not ignore the temperature. *ECS Transactions* **64** (2014) 535-547 https://doi.org/10.1149/06404.0535ecst
[25] G. R. Stafford, G.M. Haarberg. The electrodeposition of AI-Nb alloys from chloroaluminate electrolytes, *Plasmas & Ions* **1** (1999) 35-44. https://doi.org/10.1016/S1288-3255(99)80010-0
[26] C. G. Fink, D. N. Solanki. Aluminum from a Fused Chloride Bath. *ECS Transactions* **91** (1947) 203-219 https://doi.org/10.1149/1.3071777
[27] R. C. Howie, D. W. Macmillan. The electrodeposition of aluminium from molten aluminium chloride/sodium chloride. *Journal of Applied Electrochemistry* **2** (1972) 217-222. https://doi.org/10.1007/BF02354979
[28] B. Nayak, M. M. Misra. The electrodeposition of aluminium on brass from a molten aluminium chloride-sodium chloride bath. *Journal of Applied Electrochemistry* **7** (1977) 45-50. https://doi.org/10.1007/BF00615529
[29] H-M. Kan, Z-W. Wang, X-Y. Wang, N. Zhang. Electrochemical deposition of aluminum on W electrode from $AlCl_3$-NaCl melts. *Transactions of Nonferrous Metals Society of China (English Edition)* **20** (2010) 158-164 https://doi.org/10.1016/S1003-6326(09)60114-X
[30] G. R. Stafford. The electrodeposition of Al_3Ti from chloroaluminate electrolytes. *Journal of the Electrochemical Society* **141(4)** (1994) 945-953. https://doi.org/10.1149/1.2054863
[31] G. T. Cheek, W. O'Grady, S. Z. El Abedin, E. M. Moustafa, F. Endres. Electrochemical studies of magnesium deposition in ionic liquids. *ECS Transactions* **3** (2007) 269-279 https://doi.org/10.1149/1.2798670
[32] T. Watkins, A. Kumar, D. A. Buttry. Designer ionic liquids for reversible electrochemical deposition/dissolution of magnesium. *Journal of American Chemical Society* **138** (2016) 641-650 https://doi.org/10.1021/jacs.5b11031
[33] A. M. Martínez, B. Børresen, G. M. Haarberg, Y. Castrillejo, R. Tunold. Electrodeposition of magnesium from $CaCl_2$-NaCl-KCl-$MgCl_2$ melts. *Journal of the Electrochemical Society* **151** (2004) C508-C513 https://doi.org/10.1149/1.1758814
[34] B. Bøsrresen, G.M. Haarberg, R. Tunold. Electrodeposition of magnesium from halide melts-charge transfer and diffusion kinetics. *Electrochimica Acta* **42** (1997) 1613-1622 https://doi.org/10.1016/S0013-4686(96)00322-2
[35] M. Pise, M. Muduli, A. Chatterjee, B. P. Kashyap, R. N. Singh, S. S. V. Tatiparti. Instantaneous-Progressive nucleation and growth of pal ladium during electrodeposition. *Results in Surfaces and Interfaces* **6** (2022) 100044 https://doi.org/10.1016/j.rsurfi.2022.100044
[36] F. C. Walsh, M. E. Herron. Electrocrystallization and electrochemical control of crystal growth: Fundamental considerations and electrodeposition of metals. *Journal of Physics D: Applied Physics* **24** (1991) 217-225 https://doi.org/10.1088/0022-3727/24/2/019

[37] S. S. V. Tatiparti, F. Ebrahimi. Potentiostatic versus galvanostatic electrodeposition of nanocrystalline Al-Mg alloy powders. *Journal of Solid State Electrochemistry* **16** (2012) 1255-1262 https://doi.org/10.1007/s10008-011-1522-5
[38] J. L Murray, The Al−Mg (Aluminum−Magnesium) system, *Bulletin of Alloy Phase Diagrams*, **(3)** 1982, 60-74. https://doi.org/10.1007/BF02873413
[39] A. Brenner, Practical Considerations Involved in the Electrodeposition of Alloys in Electrodeposition of Alloys, Principles and Practice, Volume I, Academic Press, New York, United States of America, 1963, p.44. https://doi.org/10.1016/B978-1-4831-9808-8.50011-3